Self-assembly of *N*-heterocyclic carbenes on Au(111)

Alex Inayeh[1†], Ryan R.K. Groome[1†], Ishwar Singh[2§], Alex J. Veinot[2§], Felipe Crasto de Lima[3], Roberto H. Miwa[3], Cathleen M. Crudden[2,4*✉] & Alastair B. McLean[1*✉]

The production of ordered arrays of organic molecules on metallic surfaces by means of self-assembly is one of the most powerful methods for controlled patterning on the nanometer scale. Although the self-assembly of sulfur-based ligands has been studied for decades, the thermal and oxidative instability of these systems introduces challenges in many potential applications. In recent years, it has been shown that a new ligand class, *N*-heterocyclic carbenes (NHCs), bind to metal surfaces via a metal–carbon covalent bond, resulting in monolayers with much greater stability. However, fundamental questions surrounding self-assembly in this new ligand class remain unanswered, including the simple questions of what controls NHC orientation on the surface and under what conditions they self-assemble. Herein we describe how NHC structure, surface density, deposition temperature, and annealing temperature control mobility, thermal stability, NHC surface geometry, self-assembly, and the exact chemical nature of the surface structures. These data provide the first general set of guidelines to enable the rational design of highly ordered NHC-based monolayers. Considering that NHCs may supplant thiols as the functionalization agent of choice in a wide range of applications, a detailed understanding of their surface chemistry is crucial for the success of these next-generation monolayers.

In the almost four decades since the introduction of thiols as ligands for the formation of organic thin films on metals,[1] many of the principles of their self-assembly on gold have been elucidated.[2-8] The same cannot be said for a new type of ligand recently introduced to materials science, *N*-heterocyclic carbenes (NHCs).[9-21] NHCs have important advantages compared to thiols, including improved thermal, oxidative, and chemical robustness of their self-assembled monolayers (SAMs); higher binding energies to surfaces; and the ability to bind to reactive metals without ligand decomposition.[10-12,14,22] However, many fundamental properties of NHC-based SAMs are not well-understood, including factors controlling their preferred geometry on gold, their mobility, and their ability to self-assemble.

Several groups have addressed aspects of NHC orientation and organization, pointing to the important role of substituents on the nitrogen atoms adjacent to the carbene carbon (wingtip groups),[11,15,23-25] however a general picture of what is needed to control orientation is lacking, and the effect of these substituents on self-assembly remains unclear. Other key issues such as the nature of the bond to the surface, and the mobility of the NHC on the surface have been investigated for specific NHCs,[19] but general principles are missing. Moreover, the influence of the NHC on the underlying gold has not been examined, even though adsorbate-driven destabilization of the herringbone reconstruction is known to be important in generating adatom binding sites for thiol-based SAMs.[3,8,26-28] These key details underpin the successful use of NHC-based monolayers in virtually every application.

To address these issues, we have carried out an in-depth study of 1,3-dialkylbenzimidazol-2-ylidenes, Fig. 1(a). NHCs based on this structure have been reported in both flat-lying and upright surface geometries.[15,19,23,24] SAMs of this NHC and closely related structures are known on Au(111),[11] Cu(111),[15] Ag(111)[24] and Pt(111)[22] surfaces, on Au nanoparticles,[18,29-32] in molecular electronics,[33-35] in microcontact printing,[36] and in biosensing applications,[12,37] illustrating the generality and impact of this family of NHCs. Our study illustrates the importance of NHC structure, deposition temperature, annealing temperature, and ligand density, providing much needed information on NHC orientation, mobility, self-assembly, and adatom generation, setting out a roadmap for the preparation of high quality, densely packed self-assembled NHC monolayers with predictable and tunable properties.

[1]Department of Physics, Engineering Physics, and Astronomy, Queen's University, Kingston, Ontario, K7L 3N6, Canada. [2]Department of Chemistry, Queen's University, Kingston, Ontario, K7L 3N6, Canada. [3]Instituto de Física, Universidade Federal de Uberlândia, CP 593, 38400-902, Uberlândia, MG, Brazil. [4]Institute of Transformative Bio-Molecules (WPI-ITbM), Nagoya University, Chikusa, Nagoya, 464-8602, Japan.
✉e-mail: cruddenc@chem.queensu.ca, mcleana@queensu.ca. †§These authors contributed equally to the work.

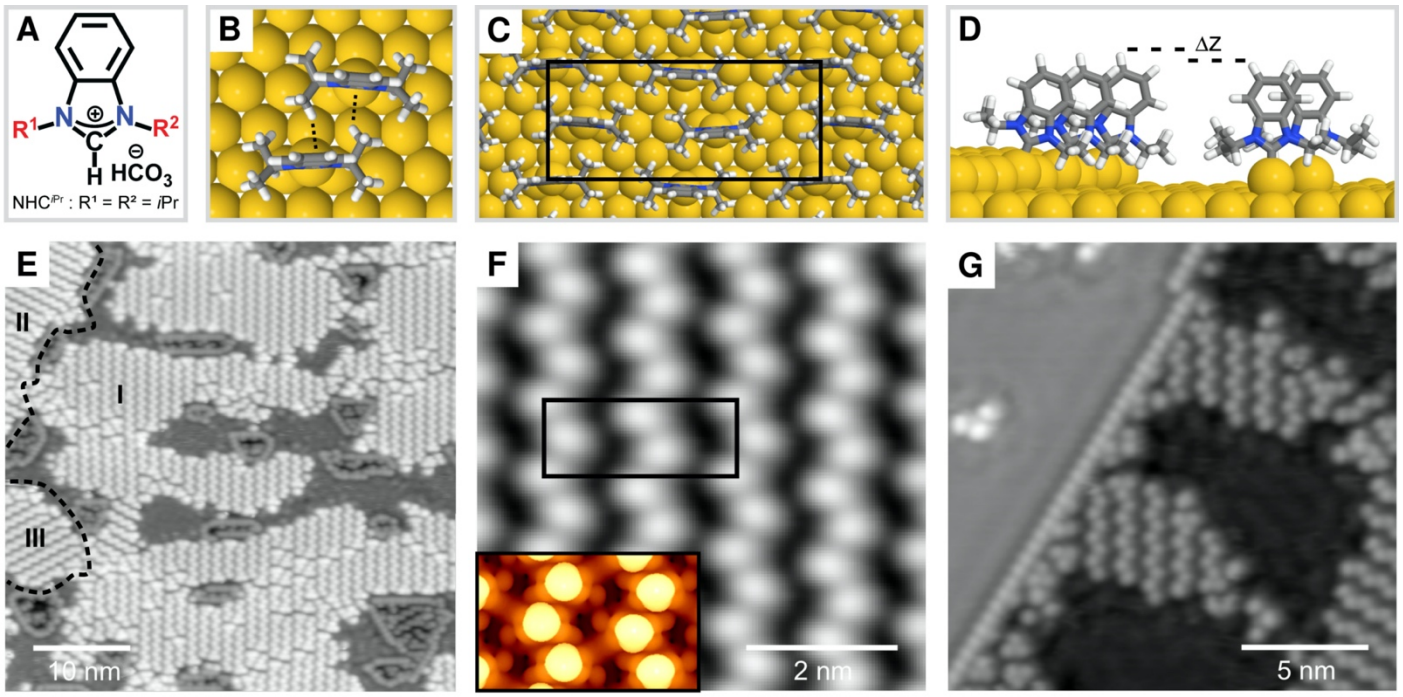

Fig. 1 | Adatom-mediated self-assembly of NHC^{iPr} into zig-zag rows stabilized by non-covalent interactions. a, Schematic structure of the bicarbonate salt. **b**, CH-π interactions between NHC^{iPr} molecules on Au(111). **c**, Model of the proposed zig-zag lattice. **d**, Model showing NHC^{iPr} molecules decorating the upper Au(111) step edge together with a zig-zag row on the lower terrace. **e**, 0.8 ML coverage of zig-zag lattice with three domains (details: 20 pA tunneling current, 100 mV sample bias, 48.0 × 48.0 nm^2 scan size, 75 °C anneal temperature). **f**, Detail of the zig-zag lattice (80 pA, 50 mV, 6.0 × 6.0 nm^2, 75 °C). The inset shows an STM simulation of the proposed zig-zag lattice. **g**, NHC^{iPr} molecules decorating the upper Au(111) step edge together with a zig-zag lattice on the lower terrace (20 pA, 100 mV, 18.0 × 18.0 nm^2, 125 °C).

NHC deposition and adatom bonding

Overlayers of NHC^{iPr} were prepared by vacuum deposition of hydrogen carbonate precursors of the general form **NHC•H_2CO_3**, Fig. 1(a), onto room temperature Au(111) substrates. The resulting surfaces were imaged by STM at 77 K, at coverages from sub-monolayer to saturation. Above 0.4 ML, NHC^{iPr} orders in zig-zag lines on terraces. This lattice, and the NHCs within it, are found to be immobile at 77 K. The study of NHC^{iPr} adsorption on Au(111) by DFT (Supplementary Figs. 1 and 2) identified the energetically preferred binding motif to be an adatom-bound NHC. Structural models based on this binding mode were validated by DFT and used to study the intermolecular forces between molecules in the lattice, Figs. 1(b-d).

Fig. 1(e) shows a surface with a zig-zag coverage of 0.8 ML that has three domains, as required by the C_{3v} symmetry of the surface. On average, the zig-zag lines are 4 nm in length, comprised of 9 molecules, and span a range of 1 to 12 nm. These zig-zag lines are accompanied by vacancy islands with depth of one atomic step, analogous to those observed in thiol self-assembly.[2,7,8] Inside these islands, NHCs self-assemble into the same zig-zag lattice.

The Au(111) herringbone reconstruction is not clearly identified under the molecular layers, which could indicate that it is significantly distorted or partially lifted by the growth of the zig-zag lattice.[26,27] In principle, the complete lifting of the herringbone reconstruction can yield up to 0.63 adatoms/nm^2.[38] However, if each NHC^{iPr} molecule in the zig-zag lattice is attached to one Au-adatom, a concentration of 1.73 adatoms/nm^2 is required to form this lattice. Since vacancy islands accompany the zig-zag lattice, these gold atoms likely originate from terraces.[2,8]

Fig. 1(f) is a high-magnification image of the zig-zag lattice, composed of upright NHC^{iPr} molecules. In matrix notation, the lattice is best described by (2,2|–8,8), with the black line in the figure defining a unit cell with dimensions (1.0 ± 0.1) nm and (2.3 ± 0.1) nm. The long side of the unit cell lies along one of the three ⟨**1 $\bar{1}$ 0**⟩ directions (Supplementary Fig. 3).

DFT simulations based upon this lattice, inset to Fig. 1(f), are in excellent agreement with experiment. The bright features are found to coincide with the aromatic ring on the NHC^{iPr} backbone, with NHC^{iPr} attached to Au-adatoms located in three-fold hollows, forming zig-zag lines, Fig. 1(c and d).

Within each line, both the NHCs and the wingtip groups tilt and rotate into favourable orientations to maximize non-covalent interactions, including: vdW, CH–π[39] and π–π.[40] The tilting of the NHCs and the rotation of their wingtip groups breaks translational symmetry, doubling the period along the line, and producing unequal zig and zag line segments in the experimental images. The contribution of the zig-zag lattice structure to the difference in line segment length is also captured by DFT (Supplementary Fig. 3).

Fig. 1(g) shows a region containing two terraces separated by a monoatomic step. NHC$^{i\mathrm{Pr}}$ molecules decorate the upper step edge, forming a one-dimensional lattice in which NHC$^{i\mathrm{Pr}}$ binds to every other gold atom. Fig. 1(d) shows the calculated conformation of NHC$^{i\mathrm{Pr}}$. The combination of relaxed steric effects and unique electronic effects at the step edge enable NHC$^{i\mathrm{Pr}}$ to adopt a purely linear conformation.

The proximity of NHC$^{i\mathrm{Pr}}$ molecules on the step edge to those on the surface below enables a direct comparison of their STM heights. The height difference, measured at a setpoint of 100 mV and 20 pA, is found to be only (72 ± 11) pm. A difference of approximately 236 pm, i.e. a single step, would be expected if the NHCs in the zig-zag lattice were attached to surface sites on the lower terrace. The observed height difference leads to the conclusion that NHC$^{i\mathrm{Pr}}$ is bound to adatoms on the lower terrace, Fig. 1(d), providing the first conclusive evidence for adatom binding.

The equilibrium structures self-assembled from NHC$^{i\mathrm{Pr}}$ are critically dependent on coverage. When NHC$^{i\mathrm{Pr}}$ is deposited on Au(111) at room temperature and below approximately 40 % of the saturation coverage, it initially binds to the high-energy adsorption sites found at upper step edges and elbows (Fig. 2(a), dotted circles) of the herringbone reconstruction,[38] and then shows a preference for FCC regions.[3,8,27] In this low coverage regime, the zig-zag lattice is not observed, however NHC$^{i\mathrm{Pr}}$ does form other lattices, shown in Fig. 2(c–f), with different packing arrangements and adatom involvement.

Comparison of the shape of the features in Fig. 2(c) with simulations leads to the conclusion that the lattice is composed only of upright NHC$^{i\mathrm{Pr}}$ molecules. Our best estimate of the matrix for the lattice shown is (3,3|–7,7).

Panel (c) also shows NHC$^{i\mathrm{Pr}}$ molecules decorating the step edge and the elbows of the herringbone reconstruction. A detailed examination of the STM-heights in this image reveals that the NHC$^{i\mathrm{Pr}}$ molecules on the terrace lie (220±10) pm below those bound on the step.

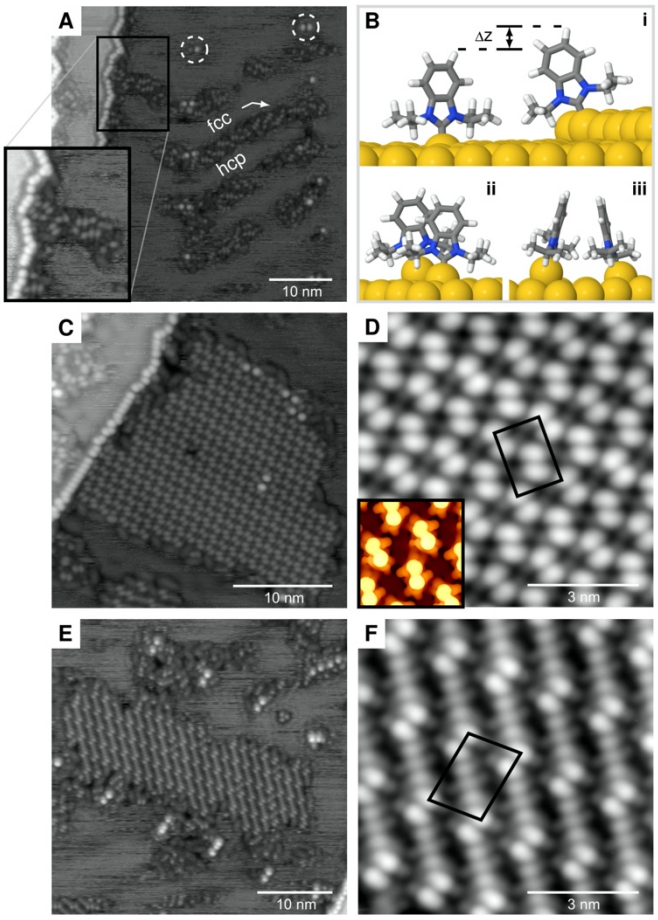

Fig. 2 | Below the critical coverage required to form zig-zag arrays, NHC$^{i\mathrm{Pr}}$ preferentially binds to surface atoms. a, In this regime, NHC$^{i\mathrm{Pr}}$ molecules preferentially occupy fcc regions of the herringbone reconstruction (20 pA, 100 mV, 48.0 × 48.0 nm^2). The inset highlights the STM height difference between NHCs attached to the step and those attached to the lower terrace. **b**, Surface binding models based on (i) calculated and simulated apparent height differences, and (ii, iii) the proposed surface-bound lattice. **c**, Array of surface-bound NHCs on Au(111) (50 pA, 400 mV, 30.0 × 30.0 nm^2). **d**, 8.0 × 8.0 nm^2 detail. **e**, Exotic lattice of mixed surface-bound NHCs and (NHC)$_2$Au complexes on Au(111) (20 pA, 100 mV, 40.0 × 40.0 nm^2). (f) 8.0 × 8.0 nm^2 detail.

This height difference, comparable to a single step, indicates that in these lattices, NHC$^{i\mathrm{Pr}}$ does not attach to gold adatoms, as it does in the zig-zag lattice, but instead attaches directly to atoms in the surface, lifting them from their equilibrium position. This is illustrated schematically in Fig. 2(b) where Δz represents the origin of the measured height difference. Using the (3,3|–7,7) matrix extracted from experimental images we performed total energy calculations, and STM simulations based on this lattice are in excellent agreement with experiment and shown in the inset to Fig. 2(d).

Fig. 2(e,f) details a more exotic lattice observed at the same low coverage regime in which upright molecules self-assemble in a dimeric structure, similar to that found in the surface-bound lattice (Fig. 2(d)), separated by flat-lying complexes with the structure $(NHC)_2Au$, where the gold complex center is lifted off the surface. This type of complex has never before been observed for NHC^{iPr}, although it has precedence in NHCs with smaller substituents.[14,15,23,24]

These three NHC^{iPr} lattices (zig-zag, surface-bound, and mixed) differ in structure and in the number of gold atoms incorporated in the overlayer. Estimated Au concentrations for the surface-bound, mixed, and zig-zag lattices are approximately 0, 0.33, and 1.73 nm^{-2}, respectively. Although the zig-zag lattice and the surface-bound lattice are immobile at 77 K, the mixed lattice is not. In STM frames taken 5–10 mins apart, structural rearrangement is commonly observed.

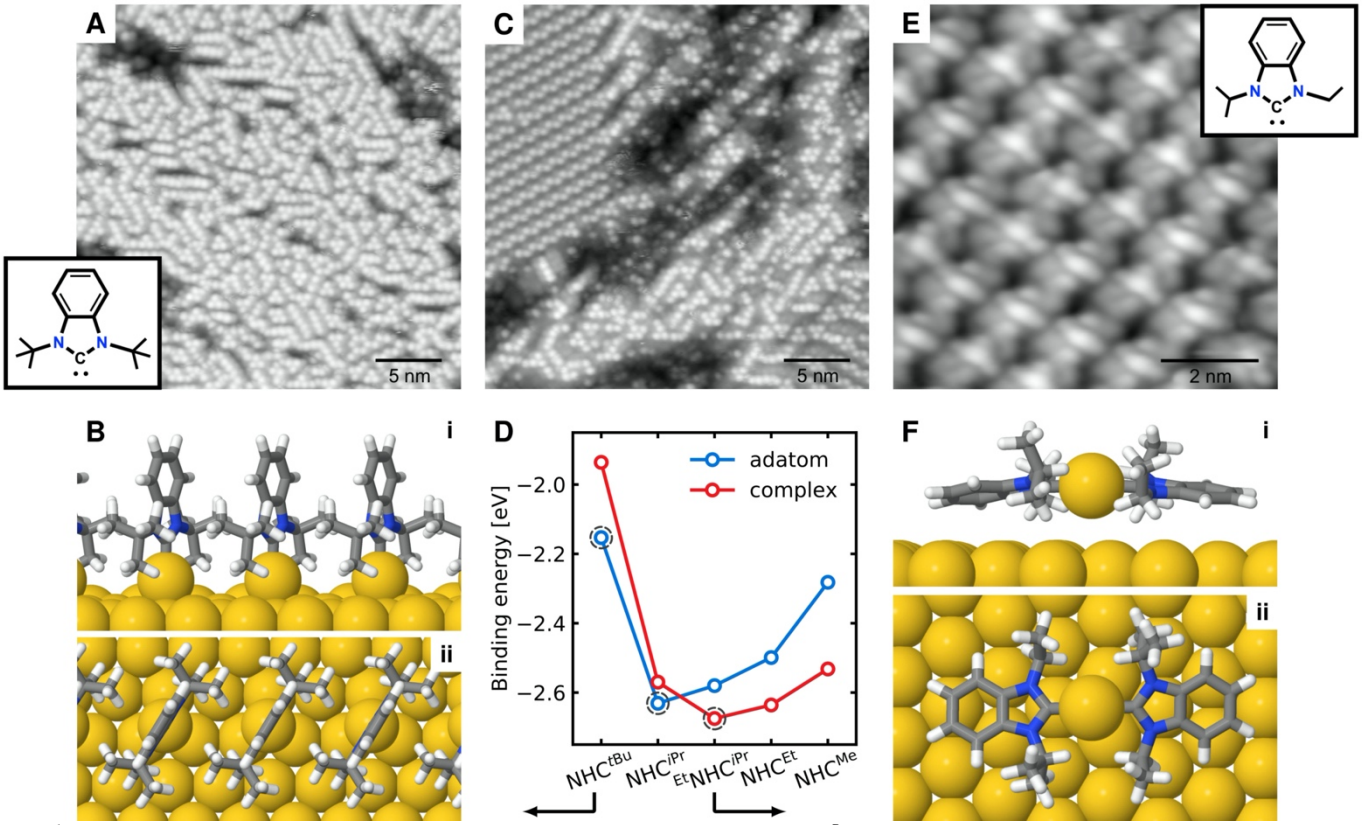

Fig. 4 | Influence of the wingtip groups on NHC binding and self-assembly. a, NHC^{tBu} self-assembles into short closely packed lines on Au(111) at saturation coverage (20 pA, 100 mV, 30.0 × 30.0 nm^2). **b**, Side and top views of NHC^{tBu} in a linear arrangement showing the adatom attachment geometry. **c**, Phase-separation of NHC^{iPr} and NHC^{tBu} molecules co-deposited in equal amounts on Au(111) (20 pA, 600 mV, 30.0 × 30.0 nm^2). **d**, Binding energy per NHC for NHC-adatom and bis-NHC complex configurations for several benzimidazole-based NHCs. **e**, $^{Et}NHC^{iPr}$ forms flat-lying $(NHC)_2Au$ complexes when deposited onto Au(111) at room temperature (30 pA, 400 mV, 8.0 × 8.0 nm^2). **f**, Side and top views of the $(NHC)_2Au$ complex centered above a three-fold hollow site.

Effect of NHC structure on orientation and order

To examine how the structure of the wingtip groups influences the self-assembly of NHC^{iPr} overlayers, we prepared and deposited structural variants of this NHC in which methyl groups are added (NHC^{tBu}), deleted ($^{Et}NHC^{iPr}$), and in which the isopropyl substituents are exhaustively deuterated (NHC^{iPr}–d_{14}).

We began with NHC^{tBu}, which was deposited onto a room temperature Au(111) surface at saturation coverage, Fig. 3(a). In the unannealed state, the NHC^{tBu} overlayer contains similar structural motifs as those formed from NHC^{iPr}, including trimers, lines and zig-zag lines (Figs 3a and 4a). However, the abundance of these structural features is different, with zig-zag lines being more abundant for NHC^{iPr} and straight lines for NHC^{tBu}. The difference is most easily illustrated using a 50:50 co-deposition on Au(111), Fig. 3(c), in which the two NHCs phase-separate.

NHC^{iPr} self-assembles into the characteristic zig-zag lattice (Fig. 3(c), top left), while NHC^{tBu} forms short lines

parallel to the three ⟨**1 $\overline{1}$ 0**⟩ directions, comprising, on average, 3-5 molecules separated by two surface lattice constants, (0.57±0.05) nm. A height difference of 56±9 pm is observed between linear NHC$^{t\mathrm{Bu}}$ chains and NHC$^{i\mathrm{Pr}}$ overlayers. Such a small difference in height is consistent with both NHC$^{i\mathrm{Pr}}$ and NHC$^{t\mathrm{Bu}}$ attaching in an upright geometry to adatoms on the surface (Fig. 3(d)). This value is well-reproduced by DFT for NHC$^{i\mathrm{Pr}}$ in the proposed zig-zag lattice and NHC$^{t\mathrm{Bu}}$ in a linear arrangement (Supplementary Fig. 4).

Unlike NHC$^{i\mathrm{Pr}}$, which shows a dramatic increase in order upon annealing, NHC$^{t\mathrm{Bu}}$ cannot be annealed to higher temperatures to increase order, due to appreciable NHC desorption between 50 and 100 °C. The NHC$^{i\mathrm{Pr}}$–Au bond is calculated to be more stable than the NHC$^{t\mathrm{Bu}}$–Au bond by a considerable amount (0.48 eV), which can in large part be attributed to the repulsive steric interactions between NHC$^{t\mathrm{Bu}}$ and the surface, introduced by the additional methyl groups.

Therefore, unlike NHC$^{i\mathrm{Pr}}$, NHC$^{t\mathrm{Bu}}$ overlayers are far from an equilibrium state, complicating any analysis of NHC$^{t\mathrm{Bu}}$ organization. By comparison, the higher level of organization observed in the NHC$^{i\mathrm{Pr}}$ overlayers likely results from the smaller *i*Pr wingtip groups, which enable the NHCs to sample a larger number of important non-covalent effects such as CH–π interactions.

To probe the effect of CH–π interactions on ordering in NHC$^{i\mathrm{Pr}}$ overlayers, we prepared NHC$^{i\mathrm{Pr}}$-d_{14}, in which both isopropyl groups were perdeuterated. The substitution of deuterium for protium is known to diminish the strength of CH–π interactions.[41] Indeed when NHC$^{i\mathrm{Pr}}$–d_{14} was deposited on Au(111), an overlayer without any long range ordering was observed (Supplementary Fig. 5). This provides conclusive evidence for the importance of CH–π effects in the self-assembly of NHC$^{i\mathrm{Pr}}$.

Structural variant $^{\mathrm{Et}}$NHC$^{i\mathrm{Pr}}$ was examined next. This NHC is related to NHC$^{i\mathrm{Pr}}$, but with a single methyl deletion. When deposited onto a room temperature surface, $^{\mathrm{Et}}$NHC$^{i\mathrm{Pr}}$ produces exclusively flat lying $(NHC)_2Au$ complexes with no upright NHCs observed, Fig. 3(e), a remarkable result considering the triviality of the structural difference. DFT comparisons of upright binding modes versus flat-lying complexes indicate that for $^{\mathrm{Et}}$NHC$^{i\mathrm{Pr}}$, bis-NHC complexes should be more stable than upright species, Fig. 3(d). These calculations also point to significant thermodynamic preferences for bis-NHC complexes with NHCs bearing methyl and ethyl wingtip groups, consistent with literature reports,[14,15,23,24] and preference for the upright geometry with NHC$^{t\mathrm{Bu}}$. Interestingly, among all NHCs examined, NHC$^{i\mathrm{Pr}}$ has the smallest energetic difference between the upright and flat-lying species, Fig. 3(d), suggesting that both should be energetically accessible.

To test for the possible interconversion of the upright and flat-lying species, overlayers of NHC$^{i\mathrm{Pr}}$ were heated above room temperature. Although NHC$^{i\mathrm{Pr}}$ self-assembles into zig-zag arrays when deposited onto Au(111) at room temperature, further annealing to 50 °C promotes an increase in order, Figs. 4(a) and (b). Remarkably, heating to only 75 °C is sufficient to convert some NHCs in the zig-zag lattice into $(NHC)_2Au$ complexes, with the relative abundance of the two phases being strongly dependent on coverage and temperature. As shown in Fig. 4(c), heating also reduces both the number and the size of the vacancy islands. This surface was heated to 100 °C and contains evidence for $(NHC)_2Au$ complexes that were captured in motion around the perimeter of the zig-zag lattice. Flat-lying $(NHC)_2Au$ complexes have never previously been observed for NHCs bearing anything but primary substituents (Me, Et, or *n*-Bu).[14,15,23,24]

At 77 K, unlike the zig-zag lattice, the complex lattice (Fig. 4(d)) is only resolvable when the complexes are spatially constrained, e.g. when the excluded surface area becomes vanishingly small, suggesting that $(NHC)_2Au$ complexes are highly mobile at this temperature. Several candidates for the experimentally observed lattice have been identified (Supplementary Table 1 and Fig. 6). We also observe the rotation of complete domains (Supplementary Fig. 7) suggesting that, at 77 K, the activation energy barriers for both complex translation and rotation are not large enough to freeze out translational and rotational changes of state.

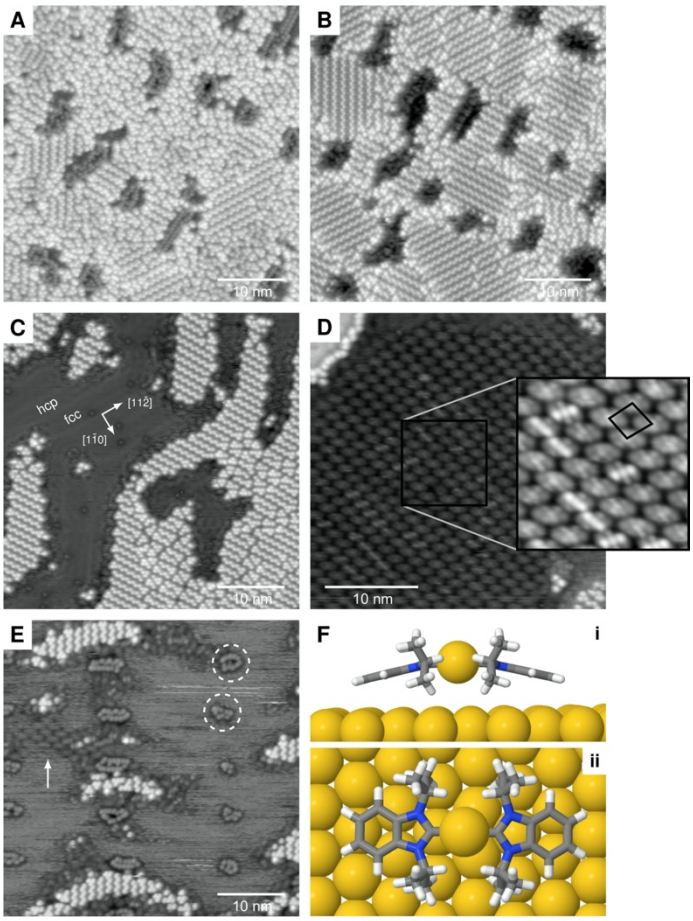

Fig. 4 | The effect of coverage and temperature on NHC^{iPr} adsorption and self-assembly on Au(111). a, Au(111) surface saturated with upright NHCs (20 pA, 100 mV, 45.0 × 45.0 nm^2). **b**, Subsequent low-temperature annealing produces highly ordered structures (50 °C, 20 pA, 100 mV, 45.0 × 45.0 nm^2). **c**, The coverage of upright species decreases when heating a saturated monolayer to 100 °C (20 pA, 100 mV, 45.0 × 45.0 nm^2). **d**, Large $(NHC)_2Au$ complex arrays form on Au(111) after heating to high temperature (140 °C, 30 pA, 100 mV, 32.0 × 32.0 nm^2). **e**, $(NHC)_2Au$ complexes form on room-temperature prepared films at low coverage and self-assemble into small, mobile arrays (20 pA, 100 mV, 45.0 × 45.0 nm^2). **f**, Side and top views of the $(NHC)_2Au$ complex.

STM images prepared at low NHC^{iPr} coverage on room temperature surfaces also contain $(NHC)_2Au$ complexes, Fig. 4(e), suggesting that these species are more ubiquitous than previously thought. In fact, only surfaces that have a saturation coverage of the zig-zag lattice are devoid of complexes, Fig. 4(a). Since complexes are mobile, they clearly play an important role in surface mass transport (Supplementary Fig. 8).

Discussion

This in-depth examination of NHC self-assembly on Au(111) enables a number of conclusions about the behaviour of NHCs on Au(111) surfaces, the stability and mobility of NHC overlayers, and the factors that control NHC speciation and surface organization.

At room temperature, and below a critical coverage, NHC^{iPr} binds primarily to surface sites, lifting surface atoms from their equilibrium positions by as much as 167 pm.[11,19,25] Above 0.4 ML, NHC^{iPr} self-assembles into trimers, lines, and a zig-zag lattice comprised of NHCs that bind exclusively to adatoms, the thermodynamically predicted attachment geometry. The abundance of the zig-zag lattice relative to other surface motifs can be increased by annealing to temperatures as low as 50 °C. This lattice is found to be stable and immobile at 77 K. The finding that a critical coverage is needed to generate the lattice is presumably related to the distortion or partial lifting of the herringbone by the well-known process of adsorbate-induced stress modification.[3,8,26-28,42] The ability of NHCs to bind to surface atoms or via adatoms is conclusively illustrated by measurements of the STM heights of NHCs on step edges as compared to those on terraces.

Both NHC^{iPr} and NHC^{tBu} bind to the surface in an upright fashion forming isomorphic structural motifs such as trimers, lines, and zig-zag rows. The effect of adding an additional methyl group is dramatic. It significantly decreases the binding energy of the NHC to the surface, preventing the system from achieving equilibrium, and restricts intramolecular rotations, complicating the ability to achieve long range order.

DFT calculations highlight the importance of CH-π interactions between the wingtip substituents and adjacent benzimidazolylidene rings and π–π interactions between the benzimidazolylidene rings. The impact of hydrogen bonding in NHC^{iPr} overlayers is clearly illustrated by deposition of the perdeuterated analogue NHC^{iPr}–d_{14}, which showed upright bonding but no long-range order.

Less sterically constrained NHCs, such as ^{Et}NHC^{iPr}, show the exclusive formation of flat-lying $(NHC)_2Au$ complexes that are mobile at 77 K. DFT calculations show that for ^{Et}NHC^{iPr}, and all other NHCs with less bulky wingtip groups, the flat-lying complex is thermodynamically preferred. This finding is of significant importance since NHCs are largely assumed to bind in an upright manner regardless of wingtip structure and the behaviour of NHCs in these two binding modes are shown to be very different.

Among those NHCs studied, NHC^{iPr} occupies a unique position, with both upright and flat-lying geometries predicted to be energetically accessible. Consequently, we observe a transition from a stable, upright, zig-zag lattice to a flat-lying $(NHC)_2Au$ complex upon annealing.

Through this study, we have demonstrated that the formation of high quality, densely packed NHC SAMs can be achieved after careful consideration of both covalent and non-covalent interactions. Differences in wingtip structure determine binding geometry, mobility, overlayer ordering, and the adatom extraction phenomenon. In

particular, wingtip groups must be large enough to disfavour flat–lying complexes, but not so large that they weaken the bond to the surface. The ability to form inter-NHC interactions and to withstand annealing is important for the formation of highly ordered, upright lattices, and the specific effect of CH–π interactions have been highlighted. These details advance the understanding of NHC-based SAMs and will be crucial to predict and control NHC SAM properties in future applications.

1. Nuzzo, R. G. & Allara, D. L. Adsorption of bifunctional organic disulfides on gold surfaces. *J. Am. Chem. Soc.* **105**, 4481-4483 (1983).
2. Poirier, G. E. Characterization of organosulfur molecular monolayers on Au(111) using scanning tunneling microscopy. *Chem. Rev.* **97**, 1117-1128 (1997).
3. Maksymovych, P., Sorescu, D. C. & Yates, J. T. Gold-adatom-mediated bonding in self-assembled short-chain alkanethiolate species on the Au(111) surface. *Phy. Rev. Lett.* **97**, 146103 (2006).
4. Yu, M. *et al.* True nature of an archetypal self-assembly system: Mobile Au-thiolate species on Au(111). *Phys. Rev. Lett.* **97**, 166102 (2006).
5. Woodruff, D. P. The interface structure of *n*-alkylthiolate self-assembled monolayers on coinage metal surfaces. *Phys. Chem. Chem. Phy.* **10**, 7211-7221 (2008).
6. Vericat, C., Vela, M. E., Benitez, G., Carro, P. & Salvarezza, R. C. Self-assembled monolayers of thiols and dithiols on gold: new challenges for a well-known system. *Chem. Soc. Rev.* **39**, 1805-1834 (2010).
7. Häkkinen, H. The gold–sulfur interface at the nanoscale. *Nat. Chem.* **4**, 443-455 (2012).
8. Maksymovych, P., Voznyy, O., Dougherty, D. B., Sorescu, D. C. & Yates, J. T. Gold adatom as a key structural component in self-assembled monolayers of organosulfur molecules on Au(111). *Prog. Surf. Sci.* **85**, 206-240 (2010).
9. Zhukhovitskiy, A. V., MacLeod, M. J. & Johnson, J. A. Carbene ligands in surface chemistry: from stabilization of discrete elemental allotropes to modification of nanoscale and bulk substrates. *Chem. Rev.* **115**, 11503-11532 (2015).
10. Smith, C. A. *et al.* N-heterocyclic carbenes in materials chemistry. *Chem. Rev.* **119**, 4986-5056 (2019).
11. Crudden, C. M. *et al.* Ultra stable self-assembled monolayers of N-heterocyclic carbenes on gold. *Nat. Chem.* **6**, 409-414 (2014).
12. Crudden, C. M. *et al.* Simple direct formation of self-assembled N-heterocyclic carbene monolayers on gold and their application in biosensing. *Nat. Comm.* **7**, 12654 (2016).
13. Engel, S., Fritz, E.-C. & Ravoo, B. J. New trends in the functionalization of metallic gold: from organosulfur ligands to N-heterocyclic carbenes. *Chem. Soc. Rev.* **46**, 2057-2075 (2017).
14. Jiang, L. *et al.* N-Heterocyclic carbenes on close-packed coinage metal surfaces: bis-carbene metal adatom bonding scheme of monolayer films on Au, Ag and Cu. *Chem. Sci.* **8**, 8301-8308 (2017).
15. Larrea, C. R. *et al.* N-heterocyclic carbene self-assembled monolayers on copper and gold: dramatic effect of wingtip groups on binding, orientation and assembly. *Chem. Phys. Chem.* **18**, 3536-3539 (2017).
16. Man, R. W. Y. *et al.* Ultrastable gold nanoparticles modified by bidentate N-heterocyclic carbene ligands. *J. Am. Chem. Soc.* **140**, 1576-1579 (2018).
17. Rühling, A. *et al.* Modular bidentate hybrid NHC-thioether ligands for the stabilization of palladium nanoparticles in various solvents. *Angew. Chem. Int. Ed.* **55**, 5856-5860 (2016).
18. Salorinne, K. *et al.* Water-soluble N-heterocyclic carbene-protected gold nanoparticles: size-controlled synthesis, stability, and optical properties. *Angew. Chem. Int. Ed.* **56**, 6198-6202 (2017).
19. Wang, G. *et al.* Ballbot-type motion of N-heterocyclic carbenes on gold surfaces. *Nat. Chem.* **9**, 152-156 (2017).
20. Weidner, T. *et al.* NHC-based self-assembled monolayers on solid gold substrates. *Aust. J. Chem.* **64**, 1177-1179 (2011).
21. Zhukhovitskiy, A. V., Mavros, M. G., Van Voorhis, T. & Johnson, J. A. Addressable carbene anchors for gold surfaces. *J. Am. Chem. Soc.* **135**, 7418-7421 (2013).
22. Zeng, Y., Zhang, T., Narouz, M. R., Crudden, C. M. & McBreen, P. H. Generation and conversion of an N-heterocyclic carbene on Pt(111). *Chem. Comm.* **54**, 12527-12530 (2018).
23. Bakker, A. *et al.* Elucidating the binding modes of N-heterocyclic carbenes on a gold surface. *J. Am. Chem. Soc.* **140**, 11889-11892 (2018).
24. Lovat, G. *et al.* Determination of the structure and geometry of N-heterocyclic carbenes on Au(111) using high-resolution spectroscopy. *Chem. Sci.* **10**, 930-935 (2019).
25. Tang, Q. & Jiang, D.-e. Comprehensive view of the ligand–gold interface from first principles. *Chem. Mater.* **29**, 6908-6915 (2017).
26. Driver, S. M., Zhang, T. & King, D. A. Massively cooperative adsorbate-induced surface restructuring and nanocluster formation. *Angew. Chem. Int. Ed.* **46**, 700-703 (2007).
27. Gao, W. *et al.* Chlorine adsorption on Au(111): chlorine overlayer or surface chloride? *J. Am. Chem. Soc.* **130**, 3560-3565 (2008).
28. Jewell, A. D., Tierney, H. L. & Sykes, E. C. H. Gently lifting gold's herringbone reconstruction: Trimethylphosphine on Au(111). *Phys. Rev. B* **82**, 205401 (2010).
29. MacLeod, M. J. & Johnson, J. A. PEGylated N-heterocyclic carbene anchors designed to stabilize gold nanoparticles in biologically relevant media. *J. Am. Chem. Soc.* **137**, 7974-7977 (2015).
30. Vignolle, J. & Tilley, T. D. N-Heterocyclic carbene-stabilized gold nanoparticles and their assembly into 3D superlattices. *Chem. Comm.*, 7230-7232 (2009).
31. Hurst, E. C., Wilson, K., Fairlamb, I. J. S. & Chechik, V. N-Heterocyclic carbene coated metal nanoparticles. *New J. Chem.* **33**, 1837-1840 (2009).
32. Rodríguez-Castillo, M. *et al.* Experimental and theoretical study of the reactivity of gold nanoparticles towards benzimidazole-2-ylidene ligands. *Chem.* **22**, 10446-10458 (2016).
33. Foti, G. & Vázquez, H. Tip-induced gating of molecular levels in carbene-based junctions. *Nanotechnology* **27**, 125702 (2016).
34. Foti, G. & Vázquez, H. Adsorbate-driven cooling of carbene-based molecular junctions. *Beilstein J. Nanotechnol.* **8**, 2060-2068 (2017).
35. Doud, E. A. *et al.* In situ formation of N-heterocyclic carbene-bound single-molecule junctions. *J. Am. Chem. Soc.* **140**, 8944-8949 (2018).
36. Nguyen, D. T. *et al.* Versatile micropatterns of N-heterocyclic carbenes on gold surfaces: increased thermal and pattern stability with enhanced conductivity. *Angew. Chem. Int. Ed.* **57**, 11465-11469 (2018).
37. DeJesus, J. F., Trujillo, M. J., Camden, J. P. & Jenkins, D. M. N-heterocyclic carbenes as a robust platform for surface-enhanced raman spectroscopy. *J. Am. Chem. Soc.* **140**, 1247-1250 (2018).
38. Barth, J. V., Brune, H., Ertl, G. & Behm, R. J. Scanning tunneling microscopy observations on the reconstructed Au(111) surface: Atomic structure, long-range superstructure, rotational domains, and surface defects. *Phys. Rev. B* **42**, 9307-9318 (1990).
39. Hudson, K. L. *et al.* Carbohydrate–aromatic interactions in proteins. *J. Am. Chem. Soc.* **137**, 15152-15160 (2015).
40. Janiak, C. A critical account on π–π stacking in metal complexes with aromatic nitrogen-containing ligands. *J. Chem. Soc., Dalton Trans.*, 3885-3896 (2000).

41. Kanao, E.; Kubo, T.; Naito, T.; Matsumoto, T.; Sano, T.; Yan, M.; Otsuka, K., Isotope effects on hydrogen bonding and CH/CD–π interaction. *J. Phys. Chem. C* **122**, 15026-15032 (2018).
42. Bach, C. E., Giesen, M., Ibach, H. & Einstein, T. L. Stress relief in reconstruction. *Phys. Rev. Lett.* **78**, 4225-4228 (1997).

Methods

With the exception of solvents, all reagents were purchased at the highest commercial quality and used without any further purification. For comprehensive experimental details-including procedures for all reactions, yields and characterization of all materials (^{1}H NMR, ^{13}C NMR, mass spectrometry, infrared spectroscopy, elemental analysis (CHN)) - see Supplementary Information.

STM measurements were performed using a CreaTec low-temperature scanning probe microscope at 77 K in UHV using the constant-current feedback mode, typically with a set current of 20 pA and a bias voltage of 100 mV.

Calculational methods are described in Supplementary Information.

Acknowledgements

A.B.M. and C.M.C. acknowledge financial support from the Natural Sciences and Engineering Research Council of Canada (NSERC) and the Canadian Foundation for Innovation (CFI). R.H.W. and F.C.dL. acknowledge financial support from the Brazilian agencies CNPq, and FAPEMIG, and the CENAPAD-SP and LNCC-SCAFMat2 for computer time. A.J.V. acknowledges NSERC for the Vanier scholarship and the Walter C. Sumner foundation for financial support.

Author Contribution

The original experiment was conceived by C.M.C. and A.B.M. but evolved in response to experimental results and discussions with all authors. I.S. and A.J.V. synthesized the NHCs. A.I. and R.R.K.G. performed the scanning probe microscopy and analyzed the experimental data. F.C.dL. and R.H.M. performed the *ab initio* calculations. A.B.M. and C.M.C. wrote the manuscript with input from all other authors.